ARTICLE NO. 79-0077R

J80-019

20005
20016
60001

Calculation of Two-Dimensional Potential Cascade Flow Using Finite Area Methods

Joseph R. Caspar,* David E. Hobbs,† and Roger L. Davis‡
United Technologies Corporation, East Hartford, Conn.

A rapid and accurate numerical method is presented for the calculation of two-dimensional potential flow in cascades. The integral form of continuity is approximated over finite areas in the physical plane, allowing the grid flexibility required by the periodicity, turning, thickness, and stagger of cascades of practical interest, and yielding second-order accuracy on appropriate meshes. Excellent agreement between predictions and analytic or measured results are shown for subsonic and transonic test cases. A model problem stability analysis supports the experimental observation that the procedure is unconditionally stable for subsonic flow and conditionally stable for transonic flow.

Nomenclature

C_P = pressure coefficient = $2(P-P_1)/\rho_1 V_1^2$
H = out-of-plane stream tube height
M = Mach number
P = pressure
r = modified isentropic density ratio, Eq. (3)
u = axial component of velocity
v = tangential component of velocity
V = magnitude of velocity, speed
γ = ratio of specific heats
θ = local flow angle measured from axial
ρ = density
τ = cascade airfoil spacing

Subscripts

$0,m$ = mesh point properties
1 = upstream properties
2 = downstream properties
T = stagnation (total) properties
x = differentiation in cascade axial direction
y = differentiation in cascade tangential direction
n = differentiation in direction normal to surface
t = differentiation in direction parallel to surface

Introduction

THIS paper describes a rapid and accurate method for calculating two-dimensional isentropic compressible potential flow in plane cascades. Cascade flow differs from isolated airfoil flow in several ways, the most important of which are that cascade flow is periodic and can be turned by the cascade. Geometrically, cascades have stagger and spacing, which are meaningless for isolated airfoils, and cascade airfoils generally are thicker and have more camber (turning) than isolated airfoils. These aspects, combined with the periodic boundary conditions, make the analysis of flow through cascades more difficult than that of flow past an isolated airfoil. Nevertheless, a fast and accurate procedure to calculate cascade flows is needed to allow the many parametric studies typically performed when a cascade airfoil section is being designed or its performance analyzed. Since geometric parameters are varied during a design, the cascade analysis must have wide geometic flexibility.

Inviscid cascade flow calculations fall into three broad types: time dependent, steady state in mapped plane, and steady state in physical plane. McDonald[1] and Denton[2] solve time-dependent Euler equations to reach steady state. These methods are not limited to potential flow, but they cannot impose all cascade boundary conditions simultaneously, and they are time consuming. Ives and Liutermoza[3,4] treat the steady-state potential equations by mapping the cascade region into a rectangle and solving the transformed equations there. This method is usually more rapid than the time-marching techniques and allows high accuracy in the range from low-speed flows to flows with embedded supersonic regions. However, it requires the extra mapping step which limits geometric flexibility, since, for example, decreasing gap (spacing) to chord ratios make cascades increasingly difficult to map.

The present analysis, which calculates potential flow properties in the physical plane, employs a nonorthogonal calculation mesh, which is easily defined for typical cascades with no gap/chord limitations and hence provides wide geometric flexibility. The difficulty of approximating the potential differential equations on a nonorthogonal mesh is avoided by approximating instead, an integro-differential form of mass conservation through "finite areas" surrounding the mesh points. This approximation is shown to be second-order accurate on appropriate meshes, despite the mesh distorting effects of stagger, turning, and thickness.

The resulting nonlinear algebraic equations are solved iteratively by calculating the potential in terms of the density and then the density in terms of the potential. This solution procedure has been found to be unconditionally stable for subsonic flow and conditionally stable for transonic flow.

Detailed information on any portion of the airfoil can be obtained by a local analysis in the region of interest using a local body fitted mesh. Such a local analysis is particularly useful in locating the leading or trailing edge stagnation points.

Received Dec. 26, 1978; presented as Paper 79-0077 at the AIAA 17th Aerospace Sciences Meeting, New Orleans, La., Jan. 15-17, 1979; revision received June 1, 1979.

Index categories: Airbreathing Propulsion; Computational Methods; Subsonic Flow.

*Senior Research Engineer, Computational Fluid Dynamics Group, United Technologies Research Center. Member AIAA.

†Research Engineer, Turbomachinery Technology, Commercial Products Division, Pratt and Whitney Aircraft Group. Member AIAA.

‡Senior Analytical Engineer, Turbomachinery Technology, Commerical Products Division, Pratt and Whitney Aircraft Group. Member AIAA.

A number of comparisons are shown between numerical predictions and analytic or measured results together with calculation times for the predictions. Calculation times vary, but the most time-consuming case shown took less than 15 s on an IBM 370/168.

Physical Model

Consider two-dimensional isentropic, compressible potential flow through a plane cascade, one passage of which is shown in Fig. 1. The direction parallel to the cascade is called the "tangential" or "y" direction, while the normal direction through the cascade is called the "axial" or "x" direction. The terms "tangential" and "axial" refer to turbomachinery coordinates. The flow is assumed known and uniform at stations 1 and 2, which are arbitrary distances upstream and downstream, respectively, of the cascade. If the trailing edge is sharp, a Kutta condition can be imposed and foreknowledge of downstream conditions eliminated.

The potential function ϕ, which exists when the flow is irrotational, satisfies

$$\phi_x = u/V_1 \quad \phi_y = v/V_1 \tag{1}$$

Given any finite area enclosed by a piecewise smooth, simply connected curve, D, ϕ must satisfy the mass balance

$$\oint_D r\phi_n \mathrm{d}s = 0 \tag{2}$$

where r is the modified isentropic density ratio,

$$r = \frac{H}{H_1}\frac{\rho}{\rho_T} = \frac{H}{H_1}\left(1 - \left[\frac{\gamma-1}{2}M_1^2\right]\Big/\left[1+\frac{\gamma-1}{2}M_1^2\right] |\nabla\phi|^2\right)^{1/(\gamma-1)} \tag{3}$$

Effects of endwall boundary layers and other sources of loss are modeled by H, which provides a quasi-three-dimensional aspect to the problem, as indicated in Fig. 1.

In addition, ϕ satisfies the boundary conditions:

Flow tangency:

$$\phi_n = 0 \text{ on the airfoil} \tag{4a}$$

Periodicity:

$$\nabla\phi(x,y+\tau) = \nabla\phi(x,y) \tag{4b}$$

Far field:

$$\phi_x, \phi_y \text{ specified and constant on stations 1 and 2} \tag{4c}$$

The derivatives ϕ_x, ϕ_y at stations 1 and 2 are obtained from knowledge of the Mach numbers M_1 and M_2 and the flow angles θ_1 and θ_2. Since these four quantities are related by global mass conservation, only three of them need to be specified. If the trailing edge is sharp, boundary condition (4c) at the downstream station may be weakened to the assumption that ϕ_x and ϕ_y are constant. The condition that ϕ_x and ϕ_y be specified is then replaced by the Kutta condition that speed be continuous at the trailing edge. In this case, M_2 and θ_2 are not specified.

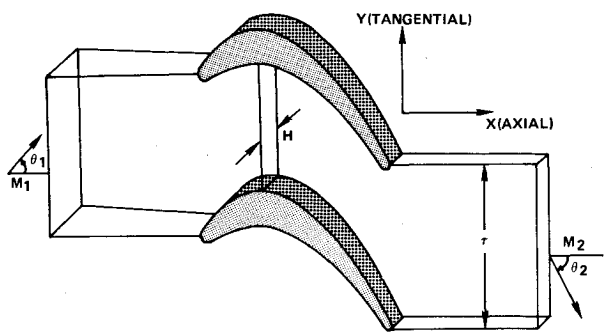

Fig. 1 Cascade passage.

Numerical Procedure

Calculation Mesh

The periodic boundary condition, Eq. (4b), imposes a very strict geometric limitation on cascade calculation meshes. In order to obtain tightly banded matrices needed for short calculation times, the mesh should be periodic, i.e., members of one family of mesh curves should begin and end either on airfoil surfaces or at points periodic to each other. Note that a mesh composed of streamlines and potential lines is not periodic, except in the unlikely case that the flow at stations 1 and 2 is axial. Conformal mapping, as used by Ives and Liutermoza,[3] can be used to produce orthogonal periodic meshes in the physical plane. However, mappings for all cascades are not presently known. The mesh employed in the analysis presented in this paper is indicated in Fig. 2. It is composed of vertical mesh lines and contour curves which are averages of the airfoil contours. It is also periodic and easily defined for typical cascade geometries and can be refined where desired. This nonorthogonal mesh easily accommodates the numerical approach that will be described later.

Finite-Area Mass Balance

The mesh is triangulated as indicated in Fig. 2 to produce, wherever possible, acute triangles. Each mesh point Q is thereby connected to a number of neighboring mesh points as shown in Fig. 3. The perpendicular bisectors of the neighbor lines are constructed forming the mesh polygon D, which sides D_m. Since the perpendicular bisectors of the sides of a triangle meet at a point, these mesh polygons exactly cover the cascade passage, i.e., each point is in one and only one mesh polygon.

Let h_m and ζ_m be the lengths, respectively, of the mth neighbor line and mth polygon side. Then Eq. (2), applied to the finite area enclosed by D, can be approximated as follows:

$$0 = \sum_m \int_{D_m} r\phi_n \mathrm{d}s \approx \sum_m \frac{r_m + r_0}{2}\frac{\phi_m - \phi_0}{h_m}\zeta_m \tag{5}$$

Because of Eq. (4a), when Q_0 is on the airfoil, the term corresponding to the polygon side through Q_0 vanishes. This finite-area approximation was first considered by MacNeal[5] to calculate an electrical potential and later by Kellogg[6] in a more general setting. To the authors' knowledge, it has not been applied previously to the velocity potential.

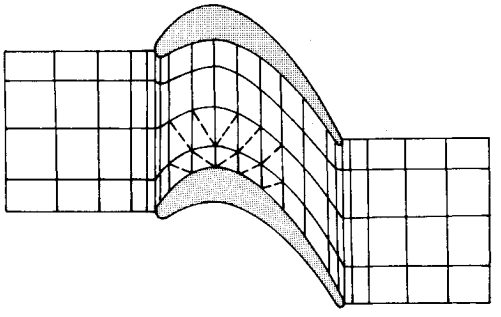

Fig. 2 Very coarse global mesh with triangulation indicated by dashed lines.

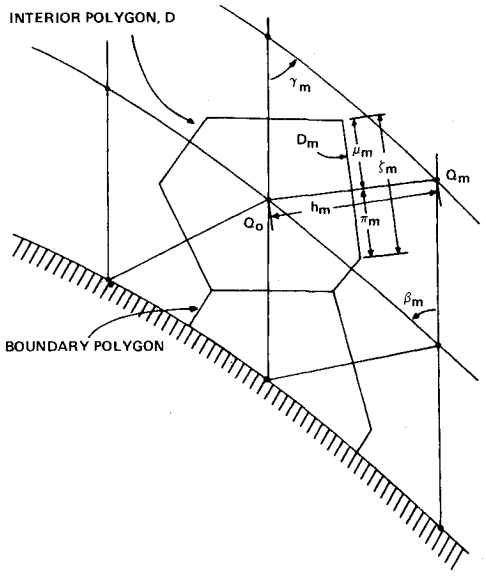

Fig. 3 Mesh polygons.

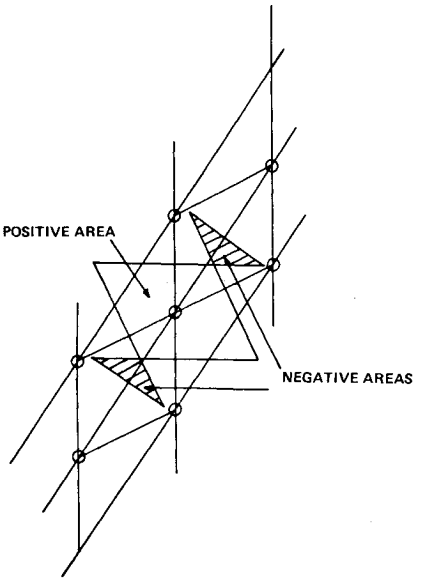

Fig. 4 Mesh polygon with negative areas.

If Eq. (5) is satisfied at each mesh point, the flow is locally conservative (continuity of mass is preserved). Moreover, since the mesh polygons cover the cascade passage, the flow is also globally conservative.

When Eq. (5) is applied on a uniform rectangular mesh, it becomes a familiar second-order approximation to the potential differential equation posed in conservation form,

$$(r\phi_x)_x + (r\phi_y)_y = 0 \tag{6}$$

which contains explicit second derivatives of ϕ. It is on a nonrectangular mesh such as that of Fig. 2, however, that the power of approximation (5) becomes clear. Because mass conservation is expressed in integral rather than differential form, only first derivatives must be approximated explicitly, and because of the form of the approximation, these derivatives are in directions determined by neighboring mesh points. This makes possible the simple approximation of Eq. (5) and avoids the problem of approximating Cartesian derivatives on a non-Cartesian mesh.

It can be shown that Eq. (5) remains second-order accurate for cascade geometries with stagger, turning, and thickness, provided the mesh is "quasiuniform" in the sense that on a given mesh line or curve, the distribution of mesh points varies smoothly. The proof of this is indicated in the Appendix. In practice, the mesh is usually refined near the airfoil and the leading and trailing edges so that it is not globally quasiuniform. However, the refinement has been found to improve accuracy despite the theoretical lower order of accuracy at the edges of the regions of refinement.

Effect of Obtuse Triangles

The length ζ_m is given by

$$\zeta_m = \pi_m + \mu_m$$

$$\pi_m = \tfrac{1}{2} h_m \cot\beta_m$$

$$\mu_m = \tfrac{1}{2} h_m \cot\gamma_m \tag{7}$$

where the lengths π_m and μ_m and the angles β_m and γ_m are indicated in Fig. 3. Clearly, if there are obtuse mesh triangles, ζ_m may be negative. This situation is illustrated in Fig. 4. The shaded regions are integrated around in a negative sense and therefore are called "negative areas."

The application of Eq. (2) to a mesh polygon with a negative area forces the mass flux through the positive area region to be the same as that through the negative area region, but it does not force the net flux to be zero. Mass conservation is maintained, however, since a nonzero mass flux through one mesh polygon is balanced by fluxes of opposite sign through adjacent polygons. Negative areas can be avoided by proper mesh refinement. However, negative areas, per se, have not been found to have a significant effect on accuracy.

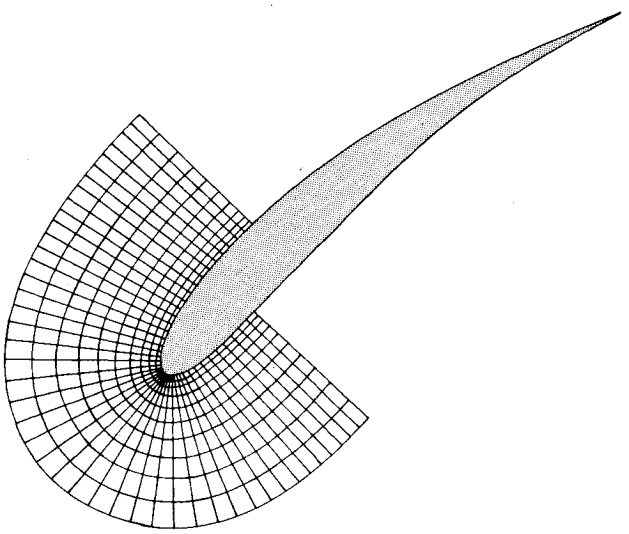

Fig. 5 Typical local mesh around leading edge.

Severe negative areas—those for which the net area of the polygon is near zero or even negative—can degrade accuracy locally. These are unlikely to occur, except at blunt leading and trailing edges where they may be caused by the unbounded mesh curve slope coupled with axial mesh refinement. Such severe negative areas can be avoided by a coarsening of the mesh, but experience indicates that the error induced by a severe negative area is less than the truncation error on a coarser mesh.

Local Analysis

The analysis on the mesh of Fig. 2 usually provides suitably accurate results even with severe negative areas at a blunt leading edge. This may not be the case, however, if very detailed results are needed about the leading edge. Such detail might be needed to predict the location of the leading-edge stagnation point or a very sharp pressure gradient. Experience

has shown that the effects of approximation errors at the leading edge are felt only a short distance from the source of the error. This makes feasible a local analysis on an orthogonal body fitted mesh such as shown in Fig. 5. Values of the potential are interpolated from the results of the first analysis (now called the global analysis) and prescribed on the fluid boundaries of the local mesh. Then the finite-area approximation is employed as in the global analysis.

If the effect of the leading-edge error in the global analysis is negligible on the local boundaries, then calculated properties from the global and local analyses should match quite well there. Experience has shown this is indeed the case if the local boundaries are placed far enough from the leading edge. In practice, the local boundaries are set by default and adjusted only if deemed necessary. Then the local analysis is used without iteration as a correction to the global analysis.

Approximation of ϕ_x and ϕ_y

Approximations to ϕ_x and ϕ_y are needed to define r using Eq. (3). On the airfoil surface, ϕ_x and ϕ_y are expressed in terms of the tangential derivative, which is approximated using neighboring mesh points on the airfoil in the usual fashion. This approximation is second order on quasiuniform meshes. Off the airfoil surface, two approximation methods have been used. In the first, ϕ is approximated in a neighborhood of a mesh point by a quadratic polynomial, which is obtained by a least-squares fit through the data at the mesh point and its eight natural neighbors. The derivatives of ϕ are then approximated by the derivatives of this quadratic. In the second method, ϕ_x and ϕ_y are expressed in terms of the derivatives of ϕ in the directions determined by the mesh curves. Approximations to these mesh derivatives are obtained in the usual fashion and are second order on quasiuniform meshes. Predicted Mach numbers on the airfoil obtained by using the two different methods on several test cases agreed to within a fraction of a percent, indicating the two methods give essentially the same results. The predictions of the test cases in this paper were obtained using the least-squares quadratic approximation.

Solution Procedure

The nonlinear system of equations arising from Eqs. (3) and (5) can be expressed as

$$A(r)\phi = b(r) \tag{8a}$$

$$r = R(\phi) \tag{8b}$$

where ϕ and r are vectors of the ϕ and r values at the mesh points respectively. The elements of the matrix A and the vector b depend on r while R is a function of ϕ. This system of equations is solved iteratively by successively fixing r and solving Eq. (8a) for ϕ, and then fixing ϕ and solving Eq. (8b) for r.

In the calculation, Eq. (8a) is replaced by the formally equivalent equation

$$A\Delta\phi = b - A\hat{\phi} \equiv \Delta b \tag{9}$$

where $\hat{\phi}$ is the previous iterate of ϕ, and $\Delta\phi$ is the correction

$$\Delta\phi = \phi - \hat{\phi} \tag{10}$$

This procedure of solving for the iterative correction rather than directly for the new iterate serves to minimize roundoff errors which scale with b for Eq. (8a) and Δb for Eq. (9). Indeed, an iteration based on Eq. (9) can be used to correct roundoff errors occurring in the numerical solution of linear systems.[7]

In addition, Eq. (8b) is replaced by the iteratively consistent equation,

$$r = \omega R(\phi) + (1-\omega)\hat{r} \tag{11}$$

where $\hat{r}$ is the previous iterate of r and ω is typically 1.5. This overrelaxation of the density has been found to accelerate convergence.

Matrix A of Eq. (10) is block tridiagonal when Eq. (4c) is applied downstream and block tridiagonal with an associated parameter connected with circulation about the airfoil when the Kutta condition is used. This system is efficiently solved using Gaussian elimination as presented by Van Dine.[8] The calculation of r is explicit and is also efficient.

The amount of time required to perform this analysis depends on many factors including: 1) the degree of compressibility (convergence of the iteration is rapid for low compressibility, since the problem is nearly linear); 2) the density of the mesh (the solution time for the linear system increases roughly linearly with the number of axial stations and cubically with the number of tangential stations); 3) the strength of the convergence criteria; 4) the use of an optional local analysis; and 5) the machine used. However, practical calculation times are short as will be seen below.

Convergence Considerations

This calculation procedure was initially developed for subsonic flow. Thus it does not, as yet, use special differencing techniques in supersonic regions. Nevertheless, it has proven remarkably accurate for a large class of transonic flows. For transonic cases, computational experience has shown that convergence slows as mesh density increases until, at some point, divergence occurs. High local Mach numbers or large decreases in Mach number (shocks) hasten the onset of divergence. However, many comparisons between prediction and analytic or measured data have demonstrated that a calculated solution, if converged, is accurate to within the truncation error of the mesh.

A model problem analysis verifies these numerical observations for the case of uniform flow between parallel lines a unit distance apart. The study shows that the calculation procedure is stable (i.e., convergent) provided that $\Delta\xi$, the grid spacing in the flow direction, satisfies

$$\Delta\xi > K\frac{M^2-1}{M} \tag{12}$$

where M is the Mach number and $K \approx 1/\pi$. The effective value of K for a nonmodel problem is yet to be determined.

When special differencing such as the artificial compressibility approximation of Hafez et al.[9] is used in the definition of r, a stability criterion similar to inequality (12) still exists, although the value of K may change. The model problem analysis and its applications, together with a discussion of why conditional stability can be obtained with essentially central differencing in supersonic regions, will be presented in a later paper.[10]

Sample Calculations

Predicted airfoil surface properties for flows through four cascades are presented with comparisons with analytic solutions or measured data. The sample cases include incompressible, subsonic and transonic flows, through compressor and turbine cascades with high and low gap to axial chord ratios. The inlet and exit conditions and gap to axial chord ratios for each of these cases are presented in Table 1.

The convergence criteria are that the maximum changes in ϕ and r, from one iterative step to the next, both be less than 5.0×10^{-4}. This indicates a minimum of two iterative steps even for linear incompressible cases. The second step, although theoretically unnecessary for incompressible cases, is useful for reducing roundoff errors.

Table 1 Aerodynamic information

Cascade	M_1	M_2	θ_1, deg	θ_2, deg	Gap axial chord	H_2/H_1
Gostelow	[a]	[a]	53.5	30.025	1.2392	1.0
Turbine	0.315	0.599	46.0	−64.58	0.9555	0.989
Hobson	0.575	0.575	46.123	−46.123	0.5259	1.0
Korn	0.700	0.5195	50.0	40.0	3.3445	1.0

[a] Incompressible.

Table 2 Calculation times

	Global analysis				Local analysis				
	No. mesh curves		No.		No. mesh curves		No.		Total
Cascade	Axial	Tangential	steps	Time[a]	Radial	Circumferential	steps	Time[a]	time[a]
Gostelow	50	10	2	3.1	45	11	1	2.4	5.5
Turbine	50	10	10	6.5	45	9	5	2.7	9.2
Hobson	50	10	11	7.0					7.0
Korn	45	11	11	7.6	61	11	10	6.9	14.5

[a] Seconds of IBM 370/168 times.

The typical global analysis mesh employs an axial mesh spacing of 4% of axial chord on the airfoil, except in the leading and trailing edges where the spacing is 1%, and a nonuniform tangential spacing which is more dense near the airfoil surfaces. The size of the calculation grid, the number of iterative steps, and the calculation time on an IBM 370/168 for the global analysis of each of these cases is presented in Table 2. For the three cases with blunt leading edges, a local analysis around the leading edge was also performed. The thickness of the local region is typically 40% of the throat and the extent along the airfoil is typically from 20% (of axial chord) on the upper side to 20% on the lower side for subsonic flows. For transonic cases with supersonic flow near the trailing edge, the local region is chosen extensive enough to contain the supersonic region. The local grid sizes, iteration counts, and timings are also given in Table 2. The maximum time of less than 15 s for a transonic case with a local analysis demonstrates the rapid speed of the procedure.

Gostelow Test Case

The compressor airfoil of Fig. 6 and the indicated incompressible hodograph solution were generated by Gostelow.[11] Comparisons of three predictions with the hodograph solution are shown. The first two predictions are the results of the global analysis with respectively coarse (4%) and fine (1%) axial mesh spacing in the leading-edge region. Both predictions compare extremely well with the hodograph solution, except in the leading edge region where coarse mesh truncation errors in the first case and severe negative area effects in the second case cause slight degradation of the accuracy. The comparisons for this case verify that mesh refinement improves accuracy, despite the introduction of severe negative areas. However, further mesh refinement in the leading-edge region would probably not yield substantially better agreement because of increasingly more severe negative area effects. Nevertheless, an essentially perfect agreement in the leading-edge region was obtained with a local analysis, as is seen in the third comparison in which the local prediction is combined with the global prediction outside the local region. Essentially the same local prediction is obtained from both global analyses showing that neither truncation error nor extreme negative area error from the leading edge has significant effect at the local region boundaries.

Inlet and exit angles as reported by Gostelow were specified in these cases. When the exit angle was unspecified and a Kutta condition employed, the predicted gas turning angle was reduced from Gostelow's by 0.77 deg, and the airfoil was unloaded slightly near the trailing edge with agreement still quite good.

Turbine Test Case

The airfoil of Fig. 7 is a turbine blade typical of modern engine design. The indicated subsonic compressible measured cascade data were taken at Pratt and Whitney by one of the authors, D. E. Hobbs. The global analysis was performed with inlet conditions assessed slightly different from those of Ref. 3 and was combined with a local analysis around the leading edge. Agreement between prediction and

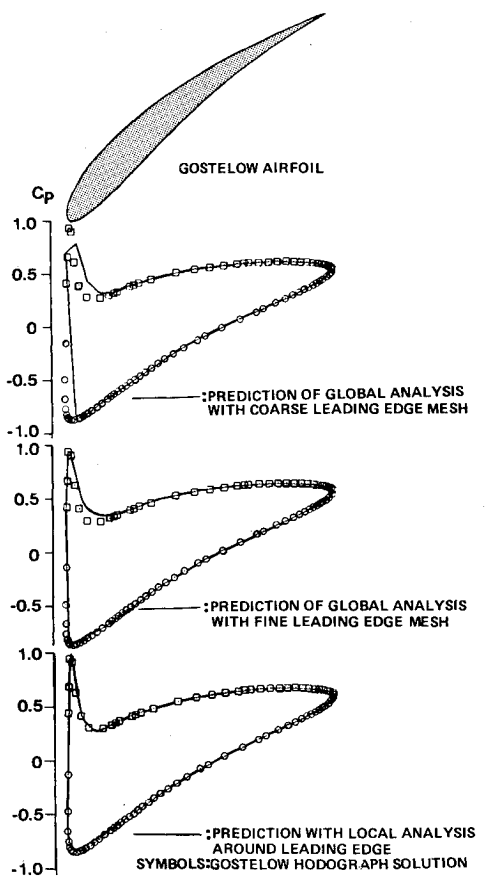

Fig. 6 Airfoil surface pressure coefficient distribution for Gostelow cascade.

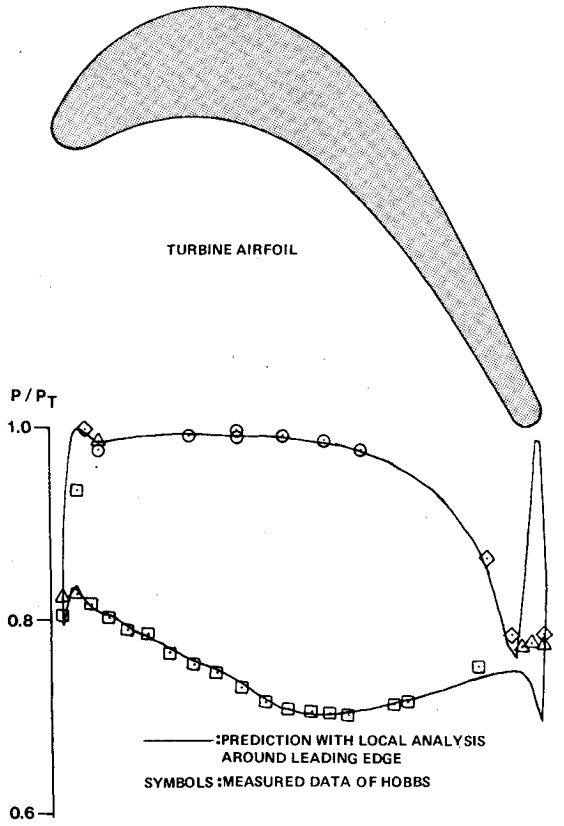

Fig. 7 Airfoil surface pressure ratio distribution for turbine cascade.

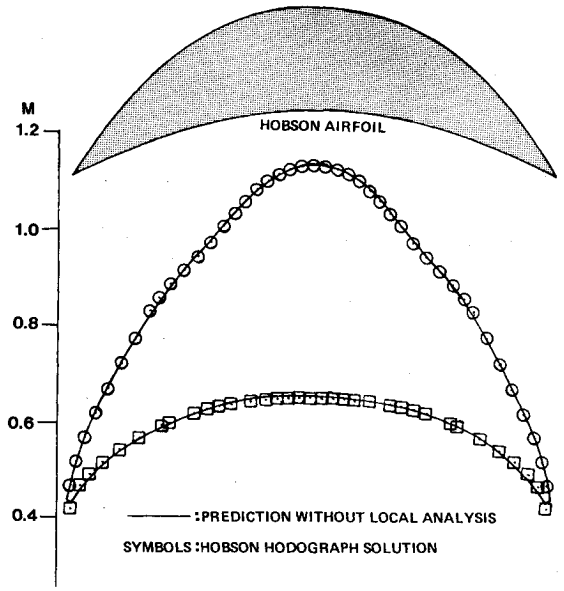

Fig. 8 Airfoil surface Mach number distribution for Hobson cascade.

measurement is remarkably good except near the inviscid trailing-edge stagnation point. This shows the usefulness of a two-dimensional potential theory to approximate actual test conditions.

Hobson Test Case

The turbine impulse airfoil of Fig. 8 and the indicated transonic hodograph solution were generated by Hobson.[12] The low gap to axial chord ratio of this cascade (0.5259) would make this cascade difficult to map. A global analysis without local analysis was performed, since the leading edge was sharp and caused no severe negative area effects. Inlet

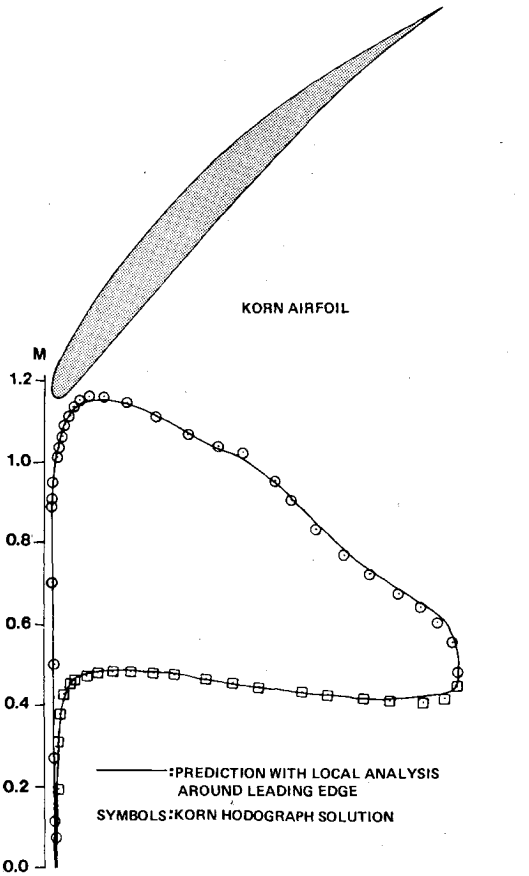

Fig. 9 Airfoil surface Mach number distribution for Korn cascade.

and exit conditions as reported by Hobson were specified. The agreement between prediction and hodograph solution is excellent, especially in the supersonic region showing that the mesh was fine enough to yield high accuracy yet coarse enough to allow convergence. When the axial density of mesh points was doubled to a 2% distribution, the iterative procedure diverged demonstrating the conditional nature of convergence for transonic flows.

Korn Test Case

The compressor airfoil of Fig. 9 and the indicated transonic hodograph solution were generated by Korn.[13] A global analysis, with inlet and exit conditions as reported by Korn, and a local analysis around the leading edge were performed. The global mesh had a 4% (of axial chord) distribution of axial mesh lines in the leading-edge region to avoid an overly dense mesh in the transonic region, and the local mesh extended from 60% on the suction side to 40% on the pressure side to assure that the local region boundaries were in regions of subsonic flow. The comparison between prediction and hodograph solutions is extremely good even in the transonic region.

Conclusions

The finite-area approximation can be applied on general nonorthogonal meshes, allowing the use of a dependably and rapidly calculated cascade mesh. The approximation is second-order accurate on quasiuniform meshes, but gives highly accurate results even on nonuniform meshes with refinement in regions of high flow gradients. The local analysis applied as a correction allows a very accurate detailed view of the flow near any portion of the airfoil. The procedure is stable for incompressible and subsonic flow and conditionally stable for transonic flow. Total calculation

times are short, making the procedure very useful in the design of cascades.

Appendix: Order of Accuracy

In this appendix, a demonstration is given that approximation (5) is second-order accurate on quasiuniform meshes, despite the mesh distorting effects of turning, stagger, and thickness. A mesh is said to be quasiuniform provided that if ΔS_1 and ΔS_2 are two successive distances between mesh points on a mesh curve, then $\Delta S_2 = \Delta S_1 + O(\Delta S_1^2)$.

For simplicity, we assume r is constant. The proof for variable r is more involved but similar. Let h be the maximum of h_m and ζ_m taken over all neighbors. Then, since the area enclosed by D is $O(h^2)$, we wish to show

$$\oint_D \phi_n \, ds = \sum_m \frac{\phi_m - \phi_0}{h_m} \zeta_m + O(h^4) \tag{A1}$$

On the mth polygon side, let t measure the distance counterclockwise along the polygon side from the neighbor line intersection. Then, expand ϕ_n in a Taylor series in t to get

$$\bar{\phi}_n = \bar{\phi}_n^m + \bar{\phi}_{nt}^m t + \tfrac{1}{2}\bar{\phi}_{ntt}^m t^2 + O(t^3)$$

where $\bar{m}$ denotes evaluation at the midpoint of the mth neighbor line and the subscript t indicates differentiation along the side. Now a Taylor series expansion in the normal direction yields

$$\bar{\phi}_n^m = \frac{\phi_m - \phi_0}{h_m} - \frac{1}{24}\bar{\phi}_{nnn}^m h_m^2 + O(h_m^4)$$

Thus,

$$\oint_D \phi_n \, ds = \sum_m \left\{ \frac{\phi_m - \phi_0}{h_m} \zeta_m + A_m + B_m + C_m \right\} + O(h^4)$$

where

$$A_m = -\frac{1}{24}\bar{\phi}_{nnn}^m h_m^2 \zeta_m$$

$$B_m = \tfrac{1}{2}\bar{\phi}_{nt}^m (\mu_m^2 - \pi_m^2)$$

$$C_m = \frac{1}{6}\bar{\phi}_{ntt}^m \zeta_m^3$$

Each of these terms is $O(h^3)$ so that Eq. (5) is formally first-order accurate on all meshes. Now, let k be the index of the neighbor opposite the mth neighbor. Then

$$|C_m + C_k| \le 1/6 |\bar{\phi}_{ntt}^m + \bar{\phi}_{ntt}^k| \, |\zeta_m^3| + 1/6 |\bar{\phi}_{ntt}^k| \, |\zeta_m^3 - \zeta_k^3|$$

If the mesh is quasiuniform, straightforward geometric and analytic arguments show that

$$|\bar{\phi}_{ntt}^m + \bar{\phi}_{ntt}^k| = O(h)$$

$$|\zeta_m^3 - \zeta_k^3| = O(h^4)$$

(Note that the kth normal is nearly the negative of the mth normal.) Thus,

$$|C_m + C_k| = O(h^4)$$

A similar result holds for the other terms so that Eq. (A1) is established and approximation (5) is second-order accurate on quasiuniform meshes.

Acknowledgments

The authors wish to acknowledge the help of R. B. Kellogg, who suggested the basic approach, and C.P. Van Dine, who took part in many fruitful discussions. They wish to thank the Commercial Products Division, Pratt and Whitney Aircraft Group, United Technologies Corporation, for its strong support of this study. They wish also to thank Ruthann Rudewicz for her patient help in putting this paper together.

References

[1] McDonald, P. W., "The Computation of Transonic Flow Through Two-Dimensional Cascades," ASME Paper 71-GT-89, Houston, Texas, March 1971.

[2] Denton, J. D., "A Time Marching Method for Two- and Three-Dimensional Blade to Blade Flows," Aeronautical Research Council, R&M No. 3775, London, Oct. 1974.

[3] Ives, D. C. and Liutermoza, J. F., "Analysis of Transonic Cascade Flow Using Conformal Mapping and Relaxation Techniques," *AIAA Journal*, Vol. 15, May 1977, pp. 647-652.

[4] Ives, D. C. and Liutermoza, J. F., "Second Order Accurate Calculation of Transonic Flow over Turbomachinery Cascades," *AIAA Journal*, Vol. 17, Aug. 1979, pp. 870-876.

[5] MacNeal, R. H., "An Asymmetrical Finite Difference Network," *Quarterly of Applied Mathematics*, Vol. XI, No. 3, Oct. 1953, pp. 295-310.

[6] Kellogg, R. B., "Difference Equations on a Mesh Arising from a General Triangulation," *Mathematics of Computation*, Vol. XVIII, No. 86, April 1964.

[7] Wilkinson, J. H., *Rounding Errors in Algebraic Processes*, Her Majesty's Stationery Office, London, 1963.

[8] Van Dine, C. P., "An Algorithm for the Optimization of Trajectories with Associated Parameters," *AIAA Journal*, Vol. 7, March 1969, pp. 400-405.

[9] Haffez, M. M., South, J. C., and Murman, E. M., "Artificial Compressibility Methods for Numerical Solution of Transonic Full Potential Equation," *AIAA Journal*, Vol. 17, Aug. 1979, pp. 838-844.

[10] Caspar, J.R., "A Model Problem Study of Transonic Potential Flow Procedures," to appear as AIAA Paper 80-0337, Pasadena, Calif., 1980.

[11] Gostelow, J. P., "Potential Flow Through Cascades—A Comparison Between Exact and Approximate Solutions," Aeronautical Research Council, London, CP No. 807, 1965.

[12] Hobson, D. G., "Shock-Free Transonic Flow in Turbomachinery Cascades," University of Cambridge, Dept. of Eng. Rept. CUED/A Turbo/TR65, 1974.

[13] Korn, D. G., "Numerical Design of Transonic Cascades," Courant Institute of Mathematical Sciences, ERDA Mathematics and Computing Laboratory, Rept. COO-3077-72, Jan. 1975.